JOURNAL OF THERMOPHYSICS AND HEAT TRANSFER
Vol. 21, No. 2, April–June 2007

Modeling of Radiation from a Side Jet Atmospheric Interaction at High Altitudes

Zheng Li,* Jiaqiang Zhong,† and Deborah A. Levin‡
Pennsylvania State University, University Park, Pennsylvania 16802

DOI: 10.2514/1.28282

Highly nonequilibrium radiation transitions from electronically excited states generated by collisions of atomic oxygen with reaction control system thruster plumes is modeled for different altitudes and vehicle velocity conditions. The flowfield results are obtained using a Navier–Stokes solver to calculate the flow inside the nozzle and the direct simulation Monte Carlo method (DSMC) is used to simulate the chemically reacting, 3-D plume-atmospheric interaction. The radiation rate is compared for two types of overlay methods and with direct simulation in DSMC. The distribution function for collisional relative velocities is explored and used to interpret the sensitivity of the radiation rate to freestream altitude, temperature, velocity, and to the radiation mechanism activation energy.

Nomenclature

A	=	Arrhenius preexponential parameter, m^3/s
B	=	Arrhenius temperature dependence parameter
$\boldsymbol{c}_a$, $\boldsymbol{c}_b$	=	Cartesian velocity vector of species a and b, m/s
E_a	=	activation energy, J
F_{num}	=	ratio of real molecules to simulated particles
$f(g)$	=	distribution function for relative collision velocities
g	=	relative collision velocity, m/s
h	=	Planck's constant, J · s
Kn	=	Knudsen number, ratio of local mean free path to the diameter of nozzle exit
k	=	Boltzmann constant, J/K
k_f	=	reaction rate, m^3/s
m_r	=	reduced mass, kg
N_r	=	radiation rate, number of radiation reactions per m^3/s
NSS	=	new species
n_k	=	number of simulated particles, per unit volume, with weighting, per m^3
n_{ts}	=	number of time steps
n'_k	=	number of atoms or molecules per unit volume, per m^3
$P(g)$	=	reaction probability
T_{ref}	=	reference temperature, K
V	=	cell volume, m^3
W_k	=	species weighting factors, where $0 < W_k \leq 1$ and k is the species index
α	=	VHS viscosity-temperature dependence parameters
Γ	=	gamma function
ϵ	=	1 for unlike species and 0 for like species, see Eq. (11)
ν	=	photon frequency, Hz
σ_r	=	reaction cross section, m^2
σ_{ref}	=	reference cross section, m^2
σ_{tot}	=	total collision cross section, m^2
τ	=	time step, s

Subscripts

FS	=	freestream
k	=	species index

I. Introduction

REACTION control system (RCS) engines are used on rockets and satellites to provide thrust for altitude maneuvers (pitch, yaw, and roll). In the past few years extensive experimental [1,2] and theoretical [3,4] studies have been undertaken to predict RCS jet interactions with the ambient atmosphere. The numerical studies were conducted at low altitudes (up to about 60 km) using solutions of the Navier–Stokes equations. At higher altitudes, the jet freestream interactions are mostly in the transitional to rarefied regimes where a continuum approach would be inapplicable to calculate the flowfield.

The direct simulation Monte Carlo (DSMC) method [5] was used in earlier work [6,7] to model the interaction between a continuum jet and the rarefied atmosphere. In the first work [6], Navier–Stokes and DSMC methods were used in the RCS nozzle and plume flow simulations. The DSMC method was used to compute the 3-D nitrogen jet interacting with freestream nitrogen for a sharp leading-edge corner flow configuration and the results were compared with experimental data. In the second work [7], a Navier–Stokes method was used to model the plume to obtain a starting surface and both Navier–Stokes and DSMC methods were used to simulate an argon plume interacting with the rarefied nitrogen freestream around a sharp leading-edge flat plate at zero incident angle. Both works simulate the jet interaction with the freestream at low altitudes where nitrogen is the main species.

For space vehicles flying through an atomic oxygen-rich environment, the interactions of the plume effluents with atomic oxygen are rare, but sufficiently energetic to cause chemical reactions of species in both ground and excited states, and radiation from excited state species potentially could interfere with onboard optical sensors. Because the plume-atmospheric interaction cannot be created in ground-based facilities, experimental validation of numerical simulations has not yet been possible. Thus, the modeling and simulation of radiation from the interaction, particularly in the ultraviolet (UV), may also provide important diagnostic information about the spatial dependence of the jet–atmosphere interaction.

The modeling of radiation from high-altitude spacecraft thruster plumes in low Earth orbit is challenging due to the multiple length scales in the plume expansion to near-vacuum conditions. The mean free path varies by five orders of magnitude from the dense plume-exit flow to the large mean free path of the freestream, ambient conditions. In our previous work [8], interaction of a jet from a side-mounted 60-lbf thruster with the rarefied atmosphere between altitudes of 80 and 160 km was modeled. The DSMC method was

Presented as Paper 3626 at the 9th AIAA/ASME Joint Thermophysics and Heat Transfer Conference, San Francisco, 5–8 June 2006; received 10 October 2006; revision received 18 January 2007; accepted for publication 19 January 2007.

*Graduate Student, Department of Aerospace Engineering. Student Member AIAA.

†Postdoctoral Fellow, Department of Aerospace Engineering. Member AIAA.

‡Associate Professor, Department of Aerospace Engineering. Associate Fellow AIAA.

applied to model the 3-D jet–atmospheric interaction with chemical reactions between freestream and plume species. The jet–atmospheric interaction structure showed significant changes for variations of the freestream altitude from 80 to 160 km. At 80 km the flowfield exhibits continuumlike features, such as an oblique shock wave, whereas at 160 km the shock is replaced by a much-diffused interaction zone. The spatial distribution of UV hydroxyl radical radiation was examined with the radiation calculation code, NEQAIR [9], and was found to follow the jet–atmospheric interaction shock structure. The previous work did not model the interaction at even higher altitudes, such as 300 km, and it is likely that similar radiation methodology cannot be used at such high altitudes. At an even higher altitude, 380 km, the modeling of ultraviolet OH(A) and NH(A) radiation from the interaction of a retrofiring hydrazine plume with the ambient atmosphere was conducted using the DSMC method [10]. An overlay [10] method was developed to examine the transient radiation phenomena for the retrofiring configuration and the 3-D steady-state radiation for a small angle of attack was calculated directly from the DSMC calculation and compared with the MirEx experimental data.

The purpose of this work is to study the nonlocal thermodynamic equilibrium (non-LTE) radiation that is caused by the interaction of reactive freestream atomic oxygen with thruster plume species. Moreover, we will show that the upper state populations cannot be modeled by an effective temperature and the actual distribution function predicted by the DSMC method must be used. Because the previous RCS–atmospheric interaction work emphasized altitudes lower than 160 km, it is unlikely that the radiation calculation employed in [9] could be applied to higher altitudes, for the same RCS configuration, because the number of collision events will be sufficiently low that it is not clear whether local thermodynamic equilibrium conditions will exist. Because of the relatively high collision velocities, there is sufficient energy to create species in electronically excited states, which can sequentially radiate. However, because there is as much as a five order of magnitude difference, for some cases, between the freestream and plume concentrations, the distribution of relative collision velocities is highly nonequilibrium. The fidelity to which these infrequent radiation events need to be modeled is difficult to quantify. Towards that end, we choose to model the radiation rate from two example systems that may occur in typical plume–atmospheric interactions: $N_2(B^3\Pi_g \rightarrow A^3\Sigma_u)$ and $OH(A^2\Sigma^+ \rightarrow X^2\Pi_i)$ radiation events, for a range of freestream conditions of 100 to 300 km and 5 to 8 km/s. Although these are not the only radiators in the ultraviolet and visible spectral regions, we chose these two systems because they have different activation energies. The main interaction between atmospheric atomic oxygen and the plume occurs in a region several meters to several hundred meters downstream of the nozzle exit where the plume expands to the rarefied atmosphere. Compared to the conditions for the calculations presented in [8], we will study the interaction at an even higher altitude, and therefore, a higher concentration of atomic oxygen. We will compare results obtained using the overlay technique developed in previous work [10] with a new numerical overlay technique that uses a distribution function based on the relative collision velocities sampled from the DSMC simulation as well as a direct modeling approach in which the radiation events are simulated in the DSMC simulations. The computational effort for these three different methods of calculating the radiative rate varies significantly, with the DSMC computation being the most intensive. The comparison of the spatial distribution of the radiation rate among the three methods will bound the uncertainty in using the less-exact methods. To study the nonequilibrium nature of the flow, we present collision relative velocity distribution functions at selected points in the flowfield and also use these results to help interpret simulation results.

The organization of the paper is as follows: In the next section, the geometry and flow conditions of the problem are presented and the potential sources of radiation are also briefly introduced. In Sec. III, the Navier–Stokes and DSMC calculation methods for flowfield as well as overlay, numerical overlay, and DSMC radiation calculation approaches are discussed. In Sec. IV, the results of jet–atmospheric interaction simulations are presented for different altitudes and vehicle velocities, and relative velocity distribution functions are shown to highlight the nonequilibrium physics of the interaction region. The three radiation calculation methods are compared and the sensitivity of the radiation rate to altitude, freestream temperature, vehicle velocity, and chemistry model are discussed.

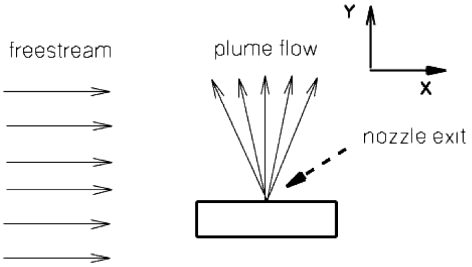

Fig. 1 Schematic of the flow.

II. Flow Conditions and Description of Problem

The schematic of the simulated flow studied in this work is shown in Fig. 1. The vehicle is modeled as a cylinder at zero angle of attack with a length of 0.3 m and a diameter of 0.06 m. A generic, bell-shaped nozzle is located on a side of the vehicle with throat and exit diameters of 0.2286 and 1.468 cm, respectively, and a length of 1.468 cm. The flow conditions at the nozzle throat and exit locations are given in Table 1. The species mole fractions at the throat are assumed to be constant throughout the nozzle. Hence we use a new species, NSS, to represent the composite effects of species CO, H_2, HCl, and CO_2. The jet species chemistry set is listed in Table 2. The mass and diameter of the composite NSS species are calculated from the mole fractions of those species given in Table 1 and assuming a hard sphere atom. The effects of this simpler chemistry model compared to a full chemistry model will be discussed in Sec. IV.D.4.

The vehicle is assumed to have a velocity of 5 or 8 km/s at an altitude of 100 or 300 km, and the freestream conditions are given in Table 3. Note that atomic oxygen is a major species in the freestream at these altitudes and the radiation reactions between freestream O atoms and the plume N_2 and H_2O molecules are the only ones considered in this work. Potential freestream–freestream and freestream–plume species chemical reactions are not included in the DSMC simulations to simplify our calculation because the contributions from such reactions to the flowfield and subsequent

Table 1 Nozzle throat and exit conditions

Parameters	Throat	Exit
Pressure, N/m^2	9.569×10^6	9291.8
Density, kg/m^3	13.0	0.04522
Temperature, K	1993.9	556.4
Mach number	1.000	5.057
N_2 mole fraction, %	13.856	——
H_2O mole fraction, %	15.621	——
CO mole fraction, %	8.157	——
H_2 mole fraction, %	26.767	——
HCl mole fraction, %	15.727	——
CO_2 mole fraction, %	19.872	——

Table 2 Nozzle throat and exit conditions

Parameters	Throat	Exit
Pressure, N/m^2	9.569×10^6	9291.8
Density, kg/m^3	13.0	0.04522
Temperature, K	1993.9	556.4
Mach number	1.000	5.057
N_2 mole fraction, %	13.856	——
H_2O mole fraction, %	15.621	——
NSS fraction, %	70.523	——

Table 3 Freestream conditions at altitudes of 100 and 300 km

Parameters		
Altitude, km	100	300
Temperature, K	184	1005
Number density, per m^3	1.100×10^{19}	8.501×10^{14}
O mole fraction, %	7	82
O_2 mole fraction, %	13	0
N mole fraction, %	0	1
N_2 mole fraction, %	80	17

Table 4 Radiation reactions[a,b]

Reagent	Product	A, m^3/s	B	E_a, J/molecule
$O + N_2$	$N_2(B) + O$	5.770×10^{-19}	0.41	1.179×10^{-18}
$O + H_2O$	$OH(A) + OH$	3.800×10^{-21}	1.30	7.674×10^{-19}

[a]Here O is from the freestream and H_2O and N_2 are from the plume.
[b]A, B, and E_a are the Arrhenius rate parameters.

radiation rate are small [11]. The two important sources of radiation come from following the transitions:

$$N_2 + O \xrightarrow{k_{f1}} N_2(B) + O \tag{1}$$

$$N_2(B) \rightarrow N_2(A) + h\nu_1 \tag{2}$$

$$H_2O + O \xrightarrow{k_{f2}} OH(A) + OH \tag{3}$$

$$OH(A) \rightarrow OH + h\nu_2 \tag{4}$$

The Arrhenius parameters for these reactions are taken from the work of Dimpfl et al. [12] and listed in Table 4. The symbols A and B in Eqs. (1–4) represent the electronic state designation for the molecular species involved in the chemiluminescent and spontaneous emission processes.

III. Numerical Method

A. Navier–Stokes Calculation

To obtain a starting surface for the DSMC calculation, the Navier–Stokes (NS) solver GASP [13] is used to obtain the relatively dense, 2-D axisymmetric flow starting from inside the nozzle throat to just outside of the nozzle exit. The computational domain, as shown in Fig. 2, extends about 0.4 m in both the plume radial X and axial Y directions. To better capture the flow gradient at the boundaries and in the shock regions, a three-zone stretched structured grid was created for the GASP/NS calculation. Zone 1, inside the nozzle, has 2500 cells, and, the exterior zones (2 and 3) each have 5000 cells.

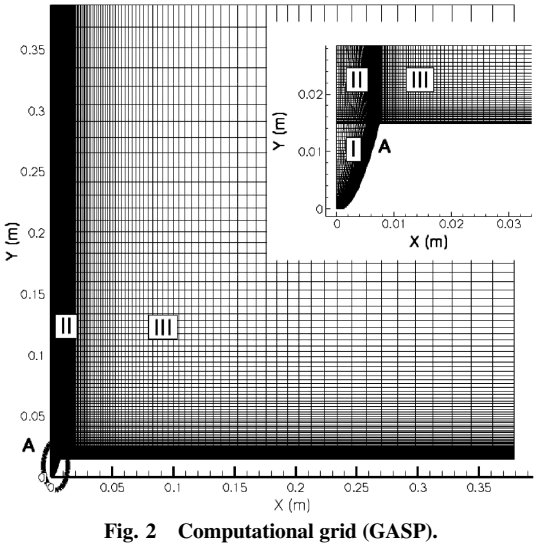

Fig. 2 Computational grid (GASP).

A no-slip boundary condition is used to model the gas–wall interactions with a fixed temperature at the rocket surface and the nozzle internal wall assumed to be 600 K. The rocket surface is the lower long boundary in Fig. 2 (between the white region and zone 3 at $Y \sim 0.015$ m) and the nozzle internal wall is the right boundary in the small inserted figure in the upper right-hand corner. The nozzle exit is assumed to be conformal to the vehicle surface. A fixed inlet boundary condition is used at the nozzle throat and first-order extrapolation boundary conditions are used at the outlets, which are the upper and right boundaries in Fig. 2. A singular boundary condition is set at the left boundary in Fig. 2 to represent an axis of symmetry.

The residence time of the flow inside the nozzle is too short for chemical reactions to occur. Therefore, to simplify the calculation, the flow is simulated as a one-species gas with an average specific heat ratio of 1.2482 and an average molecular mass of 22.515 g/mol. These two parameters are calculated from the multispecies mole fractions, given in Table 1.

B. DSMC Flowfield Calculations

In general, the use of the Navier–Stokes equations to model expansions of high density flows into a vacuum is problematic. The criteria for switching from the NS to the DSMC computational method is defined by the Knudsen number, defined as the ratio of mean free path to the characteristic length (the nozzle exit diameter). Because the NS method is valid for Knudsen numbers on the order of 0.01 and less, we analyze the NS solution to find the density contour corresponding to $Kn = 0.01$. We then construct a starting surface [8] that corresponds to a density of 3.262×10^{-4} kg/m^{-3}, or a number density of 0.873×10^{22} m^{-3}. The species number densities are calculated from the product of the starting surface densities and the mole fractions given in Table 1 because we assume that the degree of O penetration is so low that the chemistry close to the nozzle is frozen. Moreover, because the collision rate is sufficiently high close to the nozzle exit, we further assume that the velocity and temperature are the same for all species.

The DSMC-based 3-D computational tool, SMILE [14], is used in calculation. The majorant frequency scheme is employed for modeling molecular collisions. The computational domain for altitude of 300 km, shown as a solid-lined box in Fig. 3, extends 100, 200, and 40 m in the X, Y, and Z directions, with 50, 100, and 20 cells, respectively. Note that the Z direction is perpendicular to the paper. The number of subdivisions in a cell in the region near the starting surface is up to $10 \times 10 \times 10$ and the total number of collision subcells at steady state reaches approximately 0.2 million. For an altitude of 100 km, the atmospheric–plume interaction region is much smaller. Therefore, the computational domain, shown as a dashed-lined box in Fig. 3, extends only 8, 10, and 4 m in the X, Y, and Z directions, with 40, 50, and 20 cells, respectively. The number of subdivisions in a cell in the region near the starting surface is up to $20 \times 20 \times 20$ and the total number of collision subcells at steady state reaches 0.4 million.

The region designed by the symbol L shows the location of the vehicle as well as the approximate location of the starting surface discussed in the preceding section. It can be seen that the DSMC domains are much larger than the previous NS computational domain. The freestream enters the computational domain from the left boundary, and at some point starts to interact with the expanding plume, forming an interaction region where the density is increased relative to the plume and radiation reactions may occur. Based on Tables 2–4, we use nine chemical species in the DSMC simulations: N_2, O, OH, H_2O, $N_2(B)$, OH(A), NSS, O_2, and N_{2FS}. To tell the difference between freestream N_2 and plume N_2, we used two different species identifiers for them. The two radiation reactions

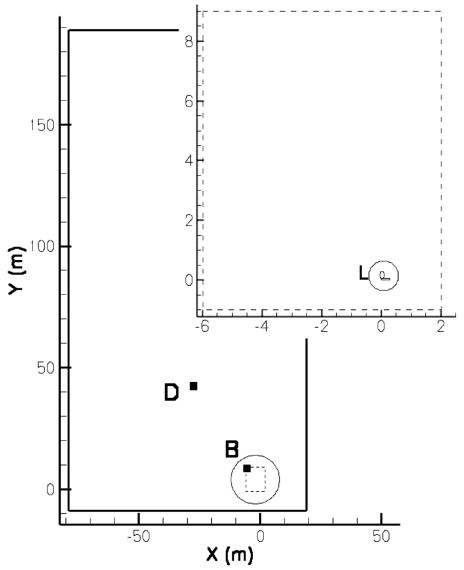

Fig. 3 DSMC calculation domains, solid-lined box for 300 km cases, dashed-lined box for 100 km cases, and symbol L points to the vehicle and starting surface.

among the plume and freestream species and the respective rate constants are summarized in Table 4.

In the DSMC calculation, to obtain good statistical results, for infrequent radiation reactions, a weighting scheme [15] is used for different species. The number of real molecules can be related to the number of simulated particles with weights by

$$n'_k = W_k F_{\text{num}} n_k \tag{5}$$

A time step of τ is chosen to keep the simulated particle distance traveled less than a grid size during one time step. The weighting factors W_k, F_{num}, and time step τ for 300 and 100 km cases are listed in Table 5. The DSMC simulation results are sampled for 500,000 steps after they reach the steady state, at the 20,000th step, with about 1.7 million simulated particles in the computational domain (at the steady state). Note that our simulation results have been examined to be independent of DSMC numerical parameters, such as time step, grid size, and number of particles. A computation typically takes about 72 h on 32 parallel AMD Athlon processors with 1.6 GHz CPUs.

C. Overlay Radiation Calculations

In the radiation calculations, the fraction of electronically excited states such as $N_2(B)$ or OH(A) that are formed is so small that they are trace species. As trace species we would not expect their presence to change the global or "bulk" flow properties such as temperature, total number density, ground-state N_2, H_2O, or freestream atomic oxygen. We will show that this is reasonable when we discuss the rate for the excitation processes given by Eqs. (1) and (3) obtained by direct calculation in DSMC. If this is the case then we can calculate the radiation reaction rates of $N_2(B)$ or OH(A) as a function of spatial location by overlaying processes (1) and (3) on the DSMC data. In this section, we assume that because the plume N_2 or H_2O number density is sufficiently high that its velocity distribution is Maxwellian.

Table 5 Time step, F_{num}, and weighting factors in DSMC calculations

Altitude	100 km	300 km
τ, s	1×10^{-6}	1×10^{-5}
F_{num}	2×10^{16}	1×10^{17}
Species	Weighting factor	
O	1×10^{-1}	1×10^{-2}
N_2	1	1
OH	1×10^{-3}	1×10^{-4}
H_2O	1	1
$N_2(B)$	1×10^{-5}	1×10^{-6}
OH(A)	1×10^{-3}	1×10^{-4}
NSS	1	1
O_2	1×10^{-1}	1×10^{-2}
N_2FS	1×10^{-1}	1×10^{-2}

According to kinetic theory, the total number of radiation reactions per second per m^3, N_r, may be expressed as

$$N_r = n_a n_b \langle \sigma_r(g) g \rangle \tag{6}$$

where n_a is the number density of reactant O species, n_b is the number density of reactant plume N_2 or H_2O species, g is the relative collision velocity between species a and b,

$$g = \sqrt{(c_{ax} - c_{bx})^2 + (c_{ay} - c_{by})^2 + (c_{az} - c_{bz})^2} \tag{7}$$

where c_{ax}, c_{ay}, c_{az}, c_{bx}, c_{by} and c_{bz} are the Cartesian velocity of species a and b. The $\langle\,\rangle$ brackets denote that the product of the collision cross section and the relative velocity should be averaged by integrating over the relative velocity g. The number densities, n_a and n_b, are obtained from the DSMC calculations described in the preceding section. The general expression for the averaged product of reaction cross section and relative collision velocity is given as

$$\langle \sigma_r(g) g \rangle = \int_0^\infty \sigma_r(g) g f(g)\, \mathrm{d}g \tag{8}$$

where $f(g)$ is the distribution function for the relative collision velocities of freestream O and plume N_2 or H_2O.

The interaction of the plume with the freestream at high altitude does not significantly affect the plume core flow because its number density is much larger than that of the freestream. Additionally, if we assume that the relative translational energy is the dominant contribution to the total collision energy (i.e., no internal energy) reaction cross section Eq. (8) may be rewritten as

$$\langle \sigma_r(g) g \rangle = \int_{-\infty}^\infty \int_{-\infty}^\infty P(g) \sigma_{\text{tot}}(g) g f(\boldsymbol{c}_a) f(\boldsymbol{c}_b)\, \mathrm{d}\boldsymbol{c}_a\, \mathrm{d}\boldsymbol{c}_b \tag{9}$$

where $P(g) = \sigma_r / \sigma_{\text{tot}}$ is the reaction probability.

For an altitude of 300 km, the N_2 or H_2O plume species temperature is relatively low compared to the freestream temperature. Therefore, we may further assume that in a given cell each of the plume N_2 molecules has the same velocity. Likewise, we assume that all plume H_2O molecules in a cell have the same velocity identical to each other. With this assumption, Eq. (9) can be simplified as

$$\langle \sigma_r(g) g \rangle = \int_{-\infty}^\infty P(g) \sigma_{\text{tot}}(g) g f(\boldsymbol{c}_a)\, \mathrm{d}\boldsymbol{c}_a \tag{10}$$

where g is now only a function of the velocity of atomic O, $\boldsymbol{c}_a$.

The standard expression for the reaction probability is given by [16] as

$$P(g) = \frac{\sigma_r}{\sigma_{\text{tot}}} = \frac{\sqrt{\pi}\epsilon A}{2\sigma_{\text{ref}}\Gamma(\frac{3}{2} + B)} \left(\frac{m_r}{2k}\right)^{\frac{1}{2}-\alpha} \left(\frac{1}{2(2-\alpha)} \frac{m_r}{kT_{\text{ref}}}\right)^{\alpha} \times \left(1 - \frac{2E_a}{m_r g^2}\right)^{1-\alpha} \left(\frac{\frac{1}{2} m_r g^2 - E_a}{k}\right)^{B-\frac{1}{2}+\alpha} \tag{11}$$

where $\epsilon = 1$ for unlike molecules and values are from [14]. The Arrhenius parameters are for the rate constant k_f,

$$k_f = A T^B \exp\left(-\frac{E_a}{kT}\right) \tag{12}$$

and are listed in Table 4.

The variable hard sphere (VHS) expression for σ_{tot} is given by [17] as

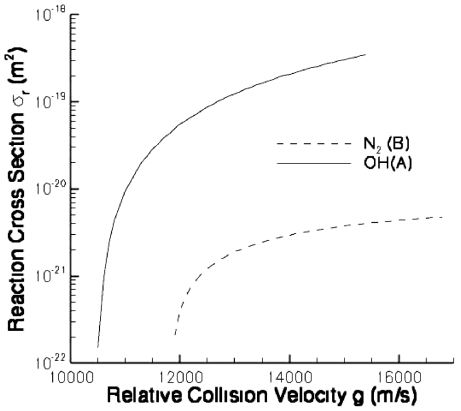

Fig. 4 Reaction cross section $\sigma_r(g)$ as a function of relative collision velocity g.

$$\sigma_{\text{tot}} = \sigma_{\text{ref}}\left(\frac{1}{2(2-\alpha)}\frac{m_r g^2}{kT_{\text{ref}}}\right)^{-\alpha} \tag{13}$$

Substitution of Eqs. (11) and (13) into Eq. (10) gives

$$N_r = n_a n_b \frac{\sqrt{\pi}\epsilon A}{\Gamma(\frac{3}{2}+B)}\left(\frac{m_r}{2k}\right)^{\frac{1}{2}-\alpha}\frac{(2-\alpha)^{1-\alpha}}{\Gamma(2-\alpha)}\int_{-\infty}^{\infty}\left(1-\frac{2E_a}{m_r g^2}\right)^{1-\alpha} \times \left(\frac{\frac{1}{2}m_r g^2 - E_a}{k}\right)^{B-\frac{1}{2}+\alpha} g^{1-2\alpha} f(\boldsymbol{c}_a)\,\mathrm{d}\boldsymbol{c}_a \tag{14}$$

where $f(\boldsymbol{c}_a) = (\frac{m_a}{2\pi k T_a})^{\frac{3}{2}}\exp(-\frac{m_a \boldsymbol{c}_a^2}{2kT_a})$ is the Maxwellian velocity distribution function and we have assumed that the oxygen atoms have an average speed and temperature throughout the flow corresponding to those in the freestream.

To evaluate Eq. (14) with the Monte Carlo method, we randomly choose 10,000 velocities in $f(\boldsymbol{c}_a)$ to obtain the average product of reaction cross section and relative collision velocity, $\langle\sigma_r(g)g\rangle$. With Eq. (14) and the velocities and densities of plume N_2 from the DSMC calculation, we can calculate the total number of radiation reactions per second per m^3, N_r. Generally, this overlay method is very fast. However, when the vehicle velocity is low, such as 5 km/s, we may have to choose so many velocities to obtain accurate results, making the calculation more time-consuming than the 8 km/s case.

D. Numerical Overlay Radiation Calculation

The expression for radiation rate, Eq. (14), is based on an assumption of an equilibrium Maxwellian distribution that may not always be valid. To obtain an accurate radiation reaction rate, we numerically integrate Eq. (8) using the actual relative velocity distribution function $f(g)$ obtained from the DSMC calculation. The reaction cross section $\sigma_r(g)$ as a function of collision velocity g can be calculated from Eqs. (11) and (13) using the Arrhenius rate coefficients of Dimpfl et al. [12] as

$$\sigma_r(g) = \frac{\sqrt{\pi}\epsilon A}{\Gamma(\frac{3}{2}+B)}\left(\frac{m_r}{2k}\right)^{\frac{1}{2}-\alpha}\left(1-\frac{2E_a}{m_r g^2}\right)^{1-\alpha} \times \left(\frac{\frac{1}{2}m_r g^2 - E_a}{k}\right)^{B-\frac{1}{2}+\alpha} g^{-2\alpha} \tag{15}$$

Figure 4 shows the resulting reaction cross sections for Eqs. (1) and (3) as a function of relative collision velocity. Because the OH(A) formation reaction has a lower threshold, the OH(A) radiation rate should be higher than that of N_2(B).

To evaluate the exact numerical overlay expression, we record the collision relative velocity distribution function $f(g)$ calculated in the DSMC calculation after sampling begins. When the calculation is finished, we normalize the relative velocities for all O and N_2 or O and H_2O pairs to obtain the distribution function of collisional relative velocity $f(g)$, as will be shown in Sec. IV.C. The reaction rate then can be numerically integrated from Eq. (8) with the reaction cross section $\sigma_r(g)$ and number densities n_a and n_b taken from the DSMC calculation. We will take two specific cells, B and D, at locations of $(-7, 7, 0)$ and $(-29, 41, 0)$ at 300 km as two examples to study the detailed distribution information. Note that because cell B is at a position nearer to plume compared to cell D, as shown in Fig. 3, we expect the velocity distributions to be significantly different.

E. Radiation Rate Obtained Directly from the DSMC Calculation

Because we have added the radiation reactions in the DSMC calculation, we can also compute the radiation rates directly. Because these rates are low, we have used small species weighting factors for N_2(B) and OH(A) to artificially increase the simulated reaction rates in the DSMC calculation (see Table 5). In each cell, we record every reaction, in each time step, after sampling with all the cases run for a total of 500,000 time steps. The reaction rate may be expressed as

$$N_r = \frac{n_r F_{\text{num}} W_k}{n_{\text{ts}}\tau V} \tag{16}$$

Because the lifetimes of N_2(B) and OH(A) in Eqs. (2) and (4) are about 1 ms [18], and therefore are on the order of the time step, the radiation rates are assumed to be the same as the reaction rates for Eq. (1) or Eq. (3). The calculation of the radiation rate in the DSMC method is the most exact method; however, it is the most difficult because the reaction is rare. Because of these conditions, we must use a large number of samples to obtain smooth results, thereby leading to long computational times.

IV. Results and Discussion

A. Flow Inside the Nozzle

The flow inside the nozzle is calculated by the Navier–Stokes solver, GASP, with the parameters and model discussed in Sec. III.A. The flow structure is shown in Fig. 5, in which density contours are plotted. The density at the center of the nozzle exit is very close to the value listed in Table 1.

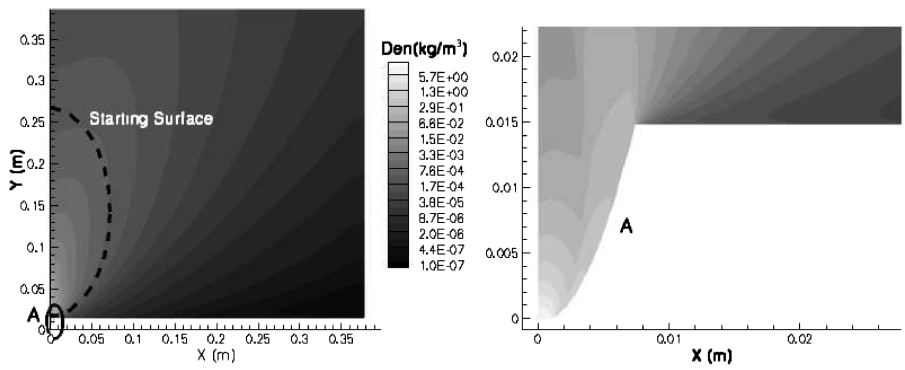

Fig. 5 Density contours from the Navier–Stokes calculation. The left-hand side shows the flowfield results over the entire NS computational domain. The right-hand side shows a zoomed region of point A, which includes the internal nozzle and near exit flowfield.

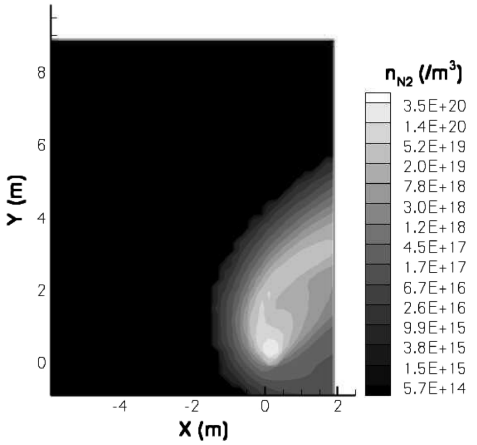

Fig. 6 Number density of plume N_2 at 100 km at a velocity of 8 km/s.

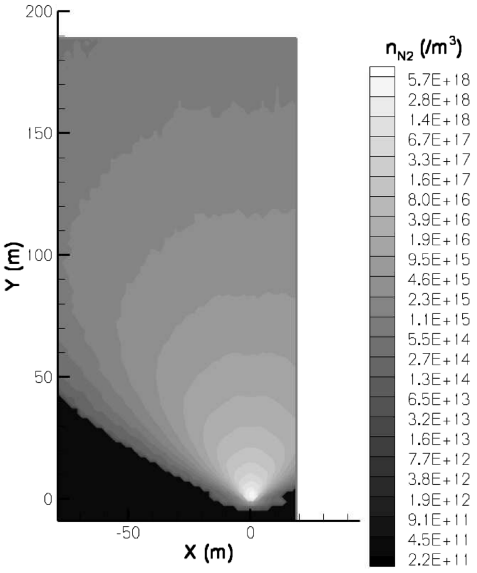

Fig. 7 Number density of plume N_2 at 300 km at a velocity of 8 km/s.

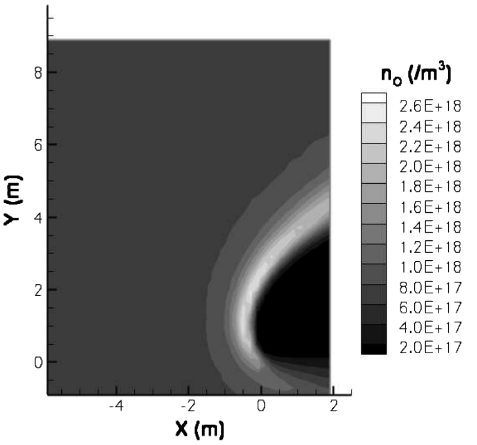

Fig. 8 Number density of freestream O at 100 km at a velocity of 8 km/s.

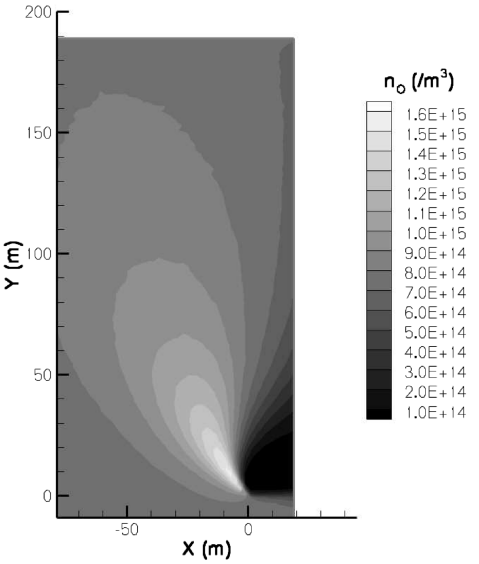

Fig. 9 Number density of freestream O at 300 km at a velocity of 8 km/s.

Because the NS method is valid for Knudsen numbers on the order of 0.01 and less, we analyze the NS solution shown in Fig. 5 to find the density contour corresponding to $Kn = 0.01$. We then construct a starting surface that corresponds to a density of 3.262×10^{-4} kg/m^{-3}. At the starting surface, the species number densities are calculated with the nozzle flow mole fractions and the velocity and temperatures are taken from the NS solution.

B. Jet/Atmosphere Interaction

Next, we consider the effect of freestream density. Figures 6 and 7 show the number density contours of plume N_2 at altitudes of 100 and 300 km with a vehicle velocity of 8 km/s. At 100 km the plume is swept back, away from the freestream because the freestream density is high and the flowfield exhibits continuumlike features. At 300 km the plume is insensitive to the freestream because there are so few collision due to low freestream density. Note the difference in the spatial range scale between the two altitudes.

Figures 8 and 9 show the number density contours of freestream O at altitudes of 100 and 300 km for a vehicle velocity of 8 km/s. At 100 km the freestream O contours skew away from the freestream, whereas at 300 km the freestream species skew towards the freestream. The variation of the atomic oxygen spatial distribution from 100 to 300 km is similar to the change in continuum-type features observed in the plume N_2 contours.

C. Examples of Velocity Distributions in the Flow

Based on the sampled DSMC data, the O species velocity distribution functions at points B (left) and D (right) in the X (top) and Y (bottom) directions are shown in Fig. 10. For both points B and D, there are two peaks in the V_x distribution function. The left peak represents those atoms that have collided with plume molecules, which leads to a lower O atom velocity, and the right peak represents those atoms that have not yet collided. Both right peaks are well fitted by Maxwellian distribution functions at a temperature of 1005 K, the freestream temperature. The corresponding V_x distribution function for point D has a higher right peak because point D is farther from the plume, which, in turn, means that there are more particles that have not collided with the plume. For point B, the V_y distribution function also has two peaks. The atoms in the right peak have collided with the plume and gain positive velocities in the Y direction. The V_y distribution function for atomic O at point D is Maxwellian because it is further from the plume.

The N_2 plume velocity distribution functions at points B (left) and D (right) for the X component of velocity are shown in Fig. 11. Both points B and D show distribution functions with negative velocity in the X direction, as the plume expands. Note that the N_2 plume number density is about four orders of magnitude greater than the O number density in this case. Thus, most of the N_2 molecules have had no chance to collide with O atoms, or other molecules, and the collisional effects seen in the O atom velocity distribution functions are not seen for plume N_2. Unlike atomic O, Fig. 11 shows that the plume N_2 velocity distribution functions are close to the equilibrium distribution functions at the local flow temperature, in all three directions at points B and D. A good fit to the Maxwellian distribution is obtained for temperatures of about 150 K or a bit less.

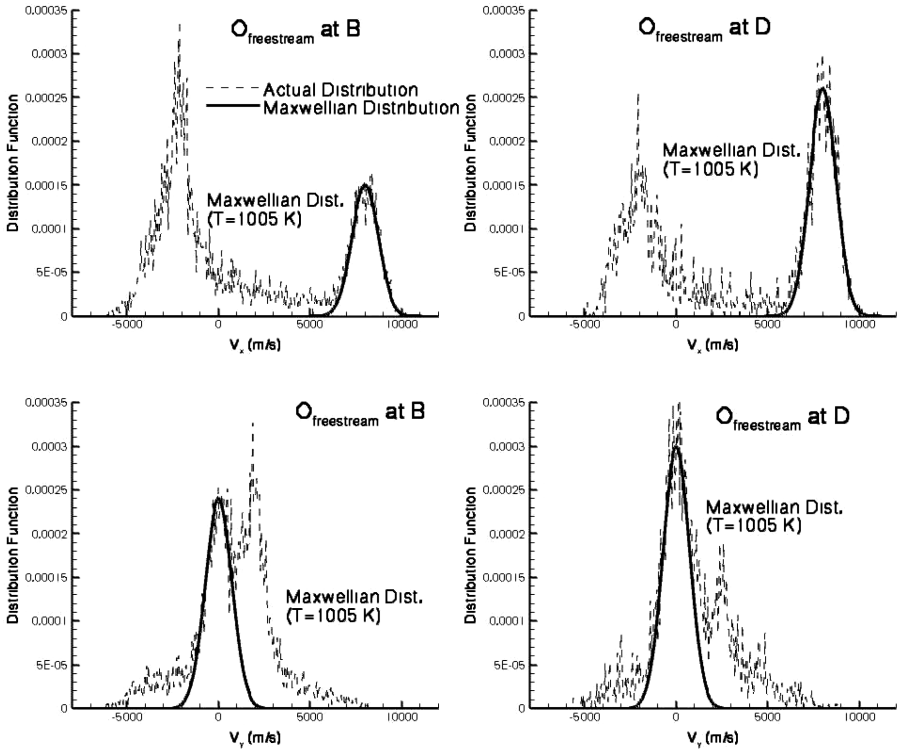

Fig. 10 Velocity distribution functions (top: X-velocity component; bottom: Y-velocity component) for freestream O at altitude of 300 km and velocity of 8 km/s. The distribution function, $f(c_a)$, is plotted on the ordinate. Here and in the subsequent figures, all the distribution functions are normalized and the dashed and solid curves represent DSMC data and the analytic Maxwellian distribution.

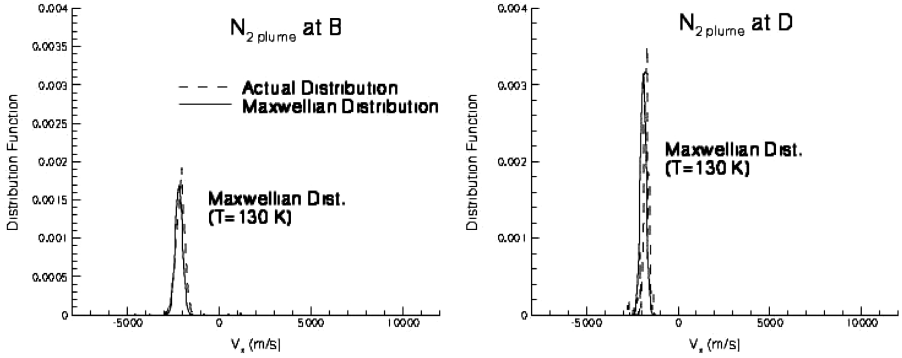

Fig. 11 Velocity distribution functions (X-velocity component) for plume N_2, $f(c_b)$, at altitude of 300 km and velocity of 8 km/s.

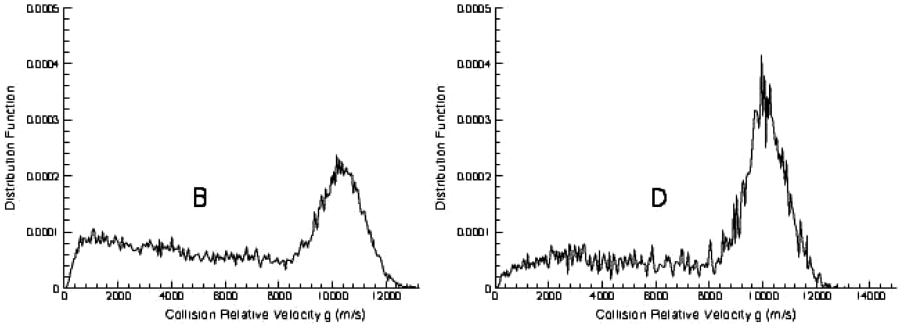

Fig. 12 Velocity distribution functions for collisional relative velocity, $f(g)$, at points B and D at altitude of 300 km and velocity of 8 km/s.

This result suggests that the plume N_2 molecules have smaller thermal velocities than the atomic O particles. The latter originate from the freestream, which has a temperature of about 1000 K. These examples demonstrate that the assumptions used in the derivative of Eq. (10), that is, the plume N_2 molecules have a fixed velocity and the oxygen atoms have an average speed and temperature throughout the flow, may be a reasonable approximation for the overlay method discussed in Sec. III.C.

The analysis of the Cartesian velocity distribution functions for particles obtained from the two different sources in this flowfield (the plume and the freestream), at two different locations, establishes credibility in the numerical task of indexing, collecting, and storing of this data. To evaluate Eq. (8) we need to know the distribution function for relative velocities of colliding O and N_2 or O and water pairs. In the DSMC calculation, we calculate the collision relative velocity, Eq. (7), and apply the acceptance and rejection principle

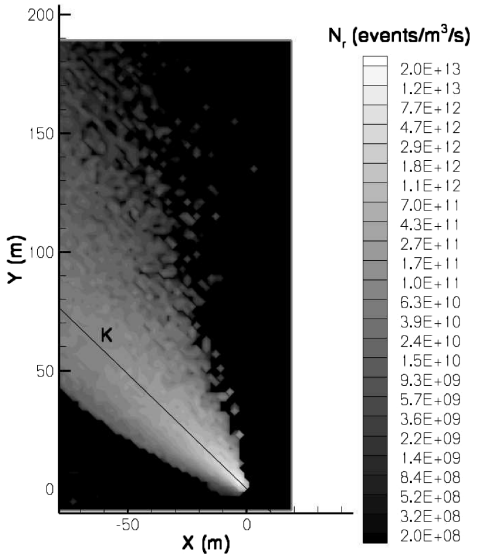

Fig. 13 Radiation rate of $N_2(B)$ from the overlay method at 300 km at a velocity of 8 km/s.

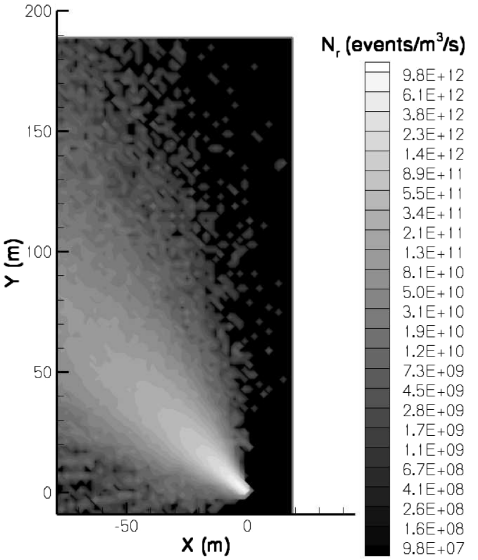

Fig. 15 Radiation rate of $N_2(B)$ from DSMC at 300 km at a velocity of 8 km/s.

[5], which ensures that the pairs selected for a collision occur with the same frequency as we would expect based on the reaction rate. Although the relative velocity distribution function is theoretically always available from DSMC calculations, in practice, it is difficult to collect and study this information due to large data storage requirements. To obtain the distribution functions of collisional relative velocity, we choose a velocity range based on the $\sigma_r(g)$–g relation in Fig. 4 and divide it into about 300 intervals. We record all the collision velocities in each cell during the DSMC calculation and bin them into the intervals and normalize the distribution function at the end of the calculation.

The normalized distribution functions for collision velocity are shown in Fig. 12. At point B, 40% of the accepted collision pairs have a collision relative velocity less than 6000 m/s, whereas at point D, the percentage of pairs with relative velocity less than 6000 m/s is 20%. This means that the reaction probability at point D is higher then point B, even though the plume number density is lower.

D. UV Radiation Rate

1. *Comparison of Different Methods*

First we consider $N_2(B)$ and OH(A) radiation at 300 km and at a velocity of 8 km/s to demonstrate the three methods for computing radiation. Figures 13–15 show the $N_2(B)$ radiation results from the overlay, numerical overlay, and DSMC methods, respectively. The spatial distribution of the radiation rate may be seen to be close, although the magnitude of the rates differ in the peak radiation region. Figure 16 shows a plot of the radiation rates predicted by the three methods on line K [from (−80, 75, 0) to (5, 0, 0)]. The rate from the overlay method is higher than the others in the region near the jet because in this overlay method we assume that all velocities follow a Maxwellian distribution and therefore none of the freestream O atoms have lost energy through collisions with plume species. This is not true, especially in region close to the jet. The rate from DSMC can be seen to be close to the numerical overlay and the residual difference is statistical error because the reaction is rare in the DSMC calculation. Figure 17 shows the corresponding OH(A) radiation results only from the overlay method because similar to the $N_2(B)$ case, the radiation rates only differ slightly among the three methods. The linear plot, Fig. 18, shows a comparison of the radiation rates from the three methods on line K. The trend is similar to the $N_2(B)$ case, with the overlay result a bit higher than the other two methods. Because the OH(A) reaction rate is higher than the $N_2(B)$ case, the curves are smoother and the DSMC result is closer to the numerical overlay method.

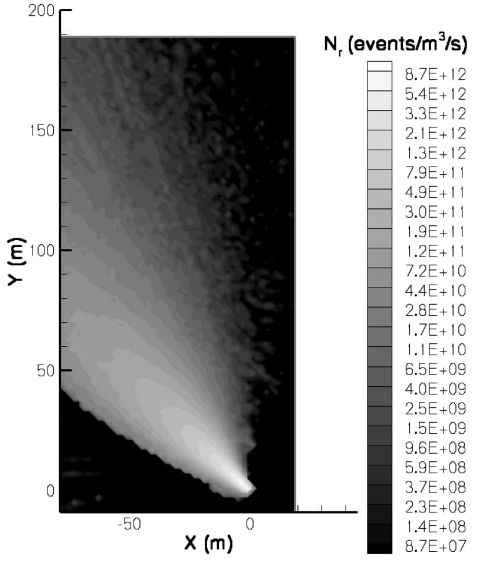

Fig. 14 Radiation rate of $N_2(B)$ from the numerical overlay method at 300 km at a velocity of 8 km/s.

2. *Sensitivity of the Radiation Rate to Altitude*

We next consider the effect of freestream number density and freestream species concentrations on the radiation. Figures 19–22

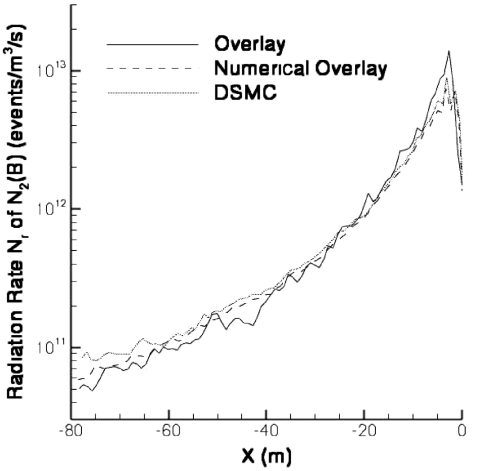

Fig. 16 Radiation rate of $N_2(B)$ from different methods on line K at 300 km at a velocity of 8 km/s. The x value of 0 is closest to the nozzle.

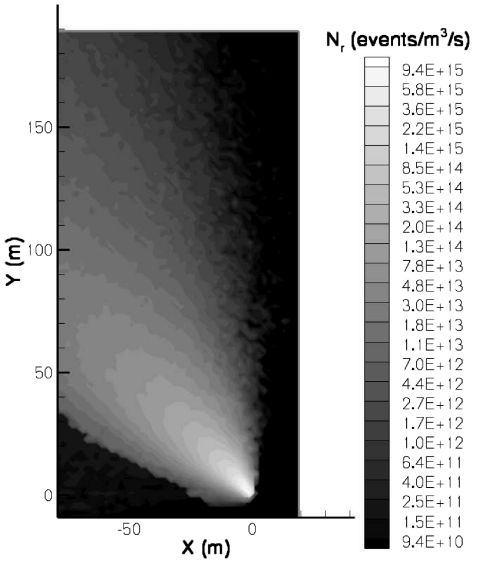

Fig. 17 Radiation rate of OH(A) from the overlay method at 300 km at a velocity of 8 km/s.

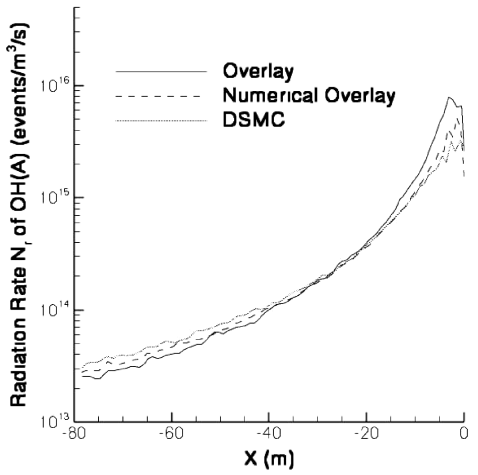

Fig. 18 Radiation rate of OH(A) from different methods on line K at 300 km at a velocity of 8 km/s.

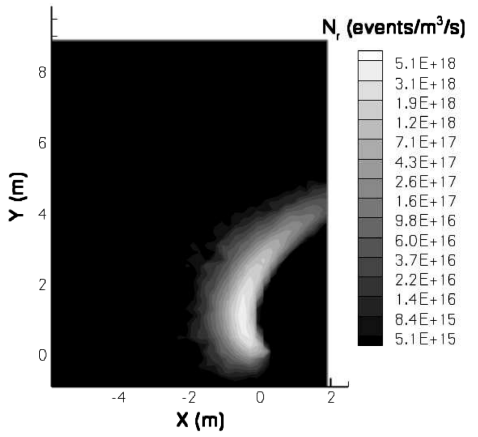

Fig. 19 Radiation rate of N_2(B) from DSMC at 100 km and a vehicle velocity of 8 km/s.

show the variation in N_2(B) and OH(A) radiation rate contours for altitudes of 100 and 300 km and for a vehicle velocity of 8 km/s. From examination of the figures, we see that because the number density of the low altitude case is higher, the radiation region is much

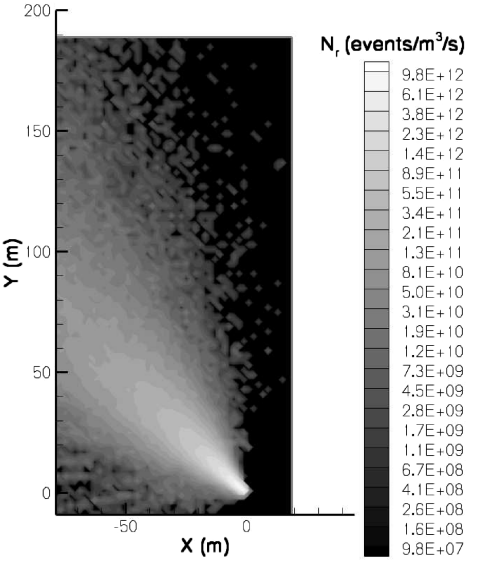

Fig. 20 Radiation rate of N_2(B) from DSMC at 300 km and a vehicle velocity of 8 km/s.

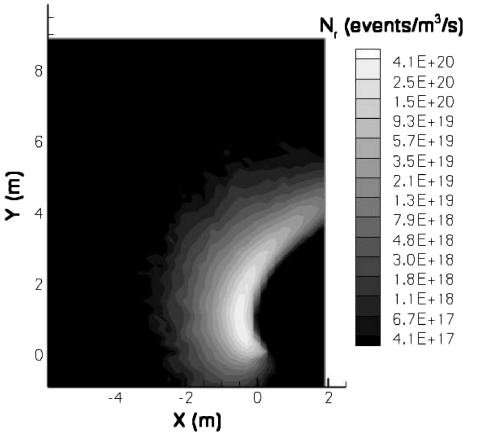

Fig. 21 Radiation rate of OH(A) from DSMC at 100 km and a vehicle velocity of 8 km/s.

smaller at 100 km than at 300 km. The ratio of the radiation at 100–300 km is found to vary by a factor of approximately 10^5, which is the ratio of the freestream number densities. For both radiation processes, the general spatial dependence is similar to that of the atomic oxygen and plume species seen earlier in Figs. 8 and 9.

3. Sensitivity of the Radiation to Freestream Temperature and Vehicle Velocity

Figure 23 shows that OH(A) radiation rate at 300 km, at a velocity of 5 km/s is predicted to be low. DSMC computations showed that for the same freestream conditions no N_2(B) radiation is predicted. To check the freestream temperature effect on the radiation field solution, we ran a special case for 300 km and 5 km/s with an artificially decreased freestream temperature of 184 K, the freestream temperature at 100 km, and found that there is no OH(A) radiation.

At point E (−29, 21, 0.0) in the flow of this special case, we sampled the collision relative velocity distribution function of plume water and freestream O. The distributions of the collisional relative velocities at point E for the original and artificially low freestream temperature cases are shown in Figs. 24 and 25. For the OH(A) radiation reaction, the critical relative velocity value,

$$V_{\text{critical}} = \sqrt{\frac{2E_a}{m_r}} \tag{17}$$

below which there are no reactions is 10, 444.3 m/s. In Fig. 24, for the low-temperature case, there are no collision pairs with a relative

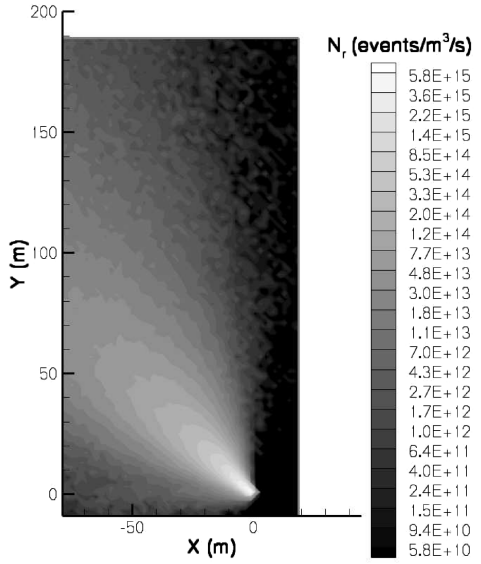

Fig. 22 Radiation rate of OH(A) from DSMC at 300 km and a vehicle velocity of 8 km/s.

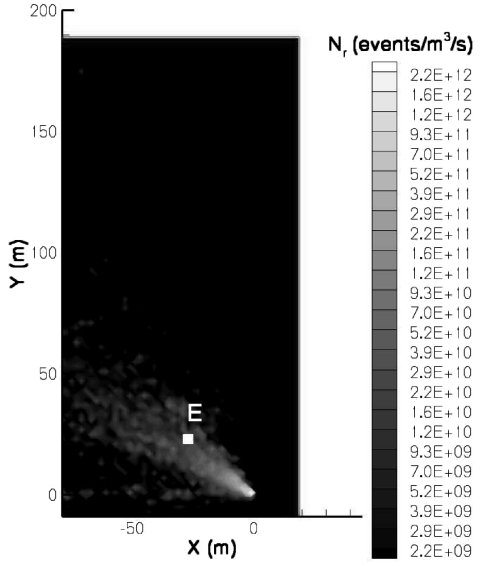

Fig. 23 Radiation rate of OH(A) from DSMC at 300 km and a vehicle velocity of 5 km/s.

velocity greater than the critical velocity and there are no radiation reactions at point E. For the original freestream temperature case, the solid curves in Fig. 24 and expanded scale in Fig. 25 show that a very small fraction of the collision pairs have velocities greater than the critical velocity. It is this small fraction of collisions that accounts for the radiation in Fig. 23. Thus for rare radiation events that may be sensitive to the tail of the distribution function, uncertainties in the freestream conditions can influence the results.

The vehicle velocity also has an important effect on the radiation rate. For a vehicle velocity of 5 km/s, there is no $N_2(B)$ radiation for the altitude of 100 km, because the relative collision velocity is too low. As a second example, consider Figs. 22 and 23, which show the OH(A) radiation rate at 300 km for 8 and 5 km/s, respectively. Compared to the 5 km/s case, the reaction probability increases dramatically and the average radiation rate is about 1000 times higher at 8 km/s.

4. *Effect of Chemistry Model*

In our calculations, we used a new species, NSS, to replace the plume species other than N_2 and H_2O. To check the effect of this replacement on the chemistry model, we simulated a case at 100 km

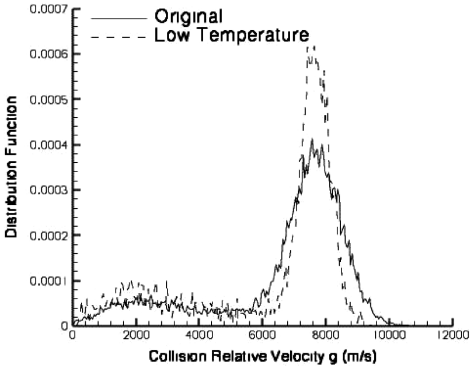

Fig. 24 Distribution functions of relative collision velocities for water and atomic O at point E at altitude of 300 km and velocity of 5 km. Solid line for original temperature case and dashed for artificially low freestream temperature case.

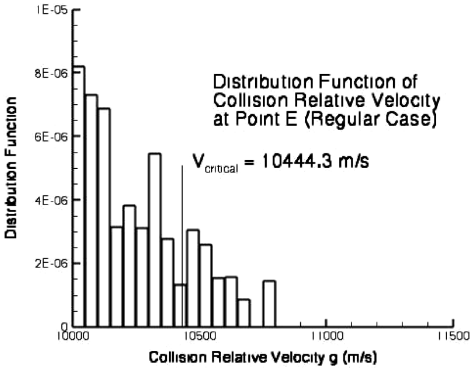

Fig. 25 Distribution function of relative collision velocity at point E for regular temperature case for an expanded velocity range corresponding to the tail of the original distribution shown in Fig. 24.

and 8 km/s with the full species set. All of the DSMC numerical parameters are the same, except that we use the NSS weighting factor for the additional CO, H_2, HCl, and CO_2 species. We choose to compare the replacement chemistry model with the full one for this freestream condition because the difference between the two models will be maximized for the range of velocities and altitudes considered in this work.

Figure 26 shows the number density contour of plume H_2O at an altitude of 100 km for a vehicle velocity of 8 km/s for the reduced species model, and Fig. 27 compares the water number density profiles for the reduced and full species model across the interaction region. The maximum difference in water concentration between the reduced species and full species model, shown in Fig. 27, is about

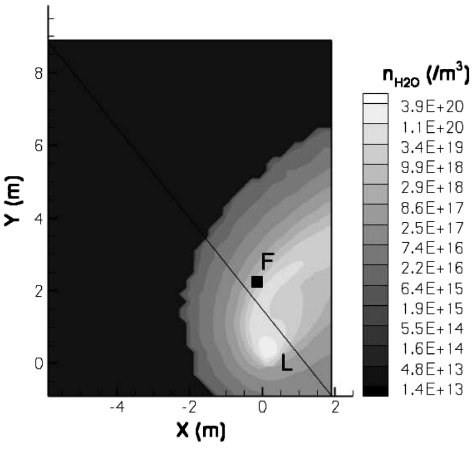

Fig. 26 Number density of H_2O at 100 km at a velocity of 8 km/s (reduced species model).

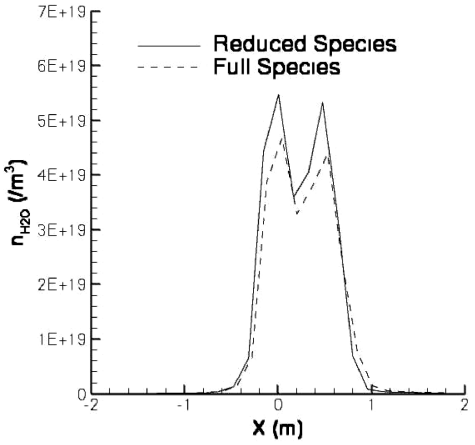

Fig. 27 Comparison of number density of H_2O at 100 km at a velocity of 8 km/s on line L.

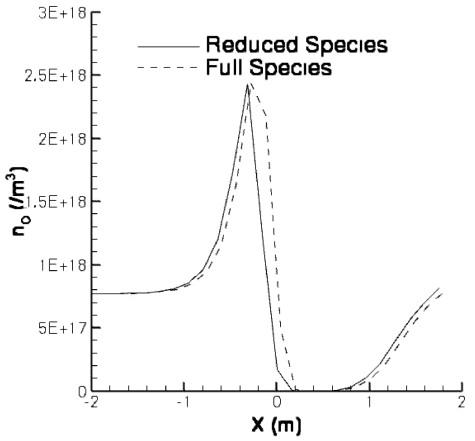

Fig. 28 Comparison of number density of O at 100 km at a velocity of 8 km/s on line L.

10%. Similarly, Fig. 28 compares the atomic oxygen profiles across the interaction region for the two reaction sets. It may be seen that the concentrations are quite close, but, the peak of the full species case is a bit wider. Figures 29 and 30 show similar profiles of translational temperatures and it may be seen that the difference is about 5%. Figure 31 shows the collision relative distribution functions for these two cases at point F (−0.3, 2.1, 0) of Fig. 26. It may be seen that the distribution function of the full species case shifts to the right, giving a higher probability of reaction. Note that unlike the relative velocity distributions at 300 km, Fig. 31 shows a single peak. The higher collision rate at the lower altitude creates a distribution function

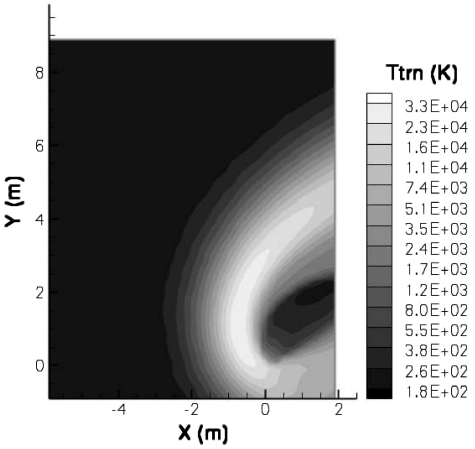

Fig. 29 Translational temperature at 100 km at a velocity of 8 km/s (reduced species model).

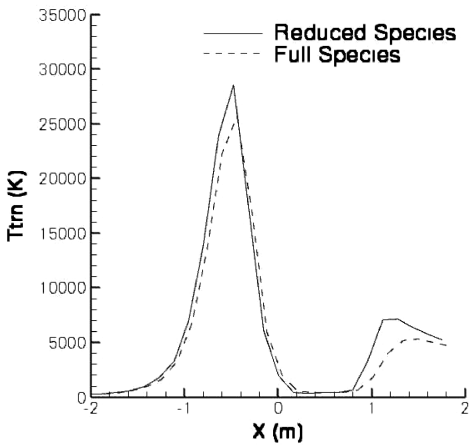

Fig. 30 Comparison of translational temperature at 100 km at a velocity of 8 km/s on line L.

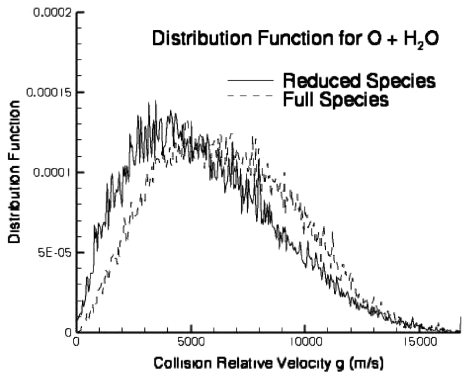

Fig. 31 Comparison of distributions at 100 km at a velocity of 8 km/s at point F.

closer to Maxwellian than was observed in Figs. 12 and 24. However, neither of the distribution functions shown in Fig. 31 are Maxwellian (values of temperature between 12,000 and 21,000 K were tried). The calculation of radiation produced by chemiluminescent reactions by use of a flowfield-derived temperature may be in error if the *tail* of the distribution dominates. This would be the case for both the OH(A) and N_2(B) radiation cases discussed in this paper because both processes have sufficiently high threshold values.

Figure 32 shows a comparison of the OH(A) radiation rates predicted by the two reaction sets, which is seen to be very close except in the peak radiation region where the difference is about 10%. This discrepancy is the resultant combination of differences in the number densities and collision relative velocities. Based on these

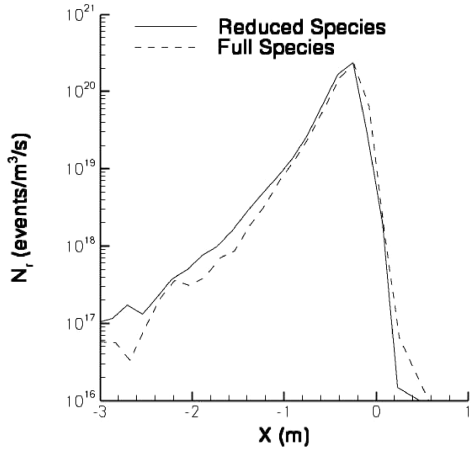

Fig. 32 Comparison of OH(A) radiation rate at 100 km at a velocity of 8 km/s.

comparisons, it may be seen that the radiation rates predicted by the reduced chemistry set are probably accurate to within 10%.

V. Conclusions

In this work, we modeled the highly nonequilibrium radiation caused by the interaction of RCS thruster plumes with reactive freestream atomic oxygen at different altitude and vehicle velocity conditions. The frequency of radiation events that are generated by the plume–atmospheric interaction from two example systems, $N_2(B)$ and OH(A), with different activation energies, were considered in our calculations.

The flow inside and near the thruster was obtained with a Navier–Stokes solver. From the NS solution, a starting surface was created to begin the DSMC calculations. The chemically reacting 3-D plume–atmosphere interacting flow outside the nozzle flow was simulated by the direct simulation Monte Carlo method. The flow was found to exhibit continuumlike features at 100 km, whereas at 300 km the plume shape was found to be relatively insensitive to the freestream.

Distributions of relative collision velocities were shown for the plume N_2 and freestream atomic O species at two different locations at 300 km with a vehicle velocity of 8 km/s. The distributions showed that there are two populations of oxygen atoms, those that have and have not collided with the plume and therefore the oxygen atom distribution function is non-Maxwellian. The ratio of O atoms that have collided with plume molecules to those that have not was found to be higher at the point closer to the plume, as expected. The velocities of the group of oxygen atoms that had not collided with the plume could be fit by a Maxwellian distribution function with a temperature corresponding to that of the freestream. As expected, the results showed that the plume N_2 species has a lower temperature or smaller thermal velocities than the atomic O particles.

Radiation rates from the three methods, overlay, numerical overlay, and DSMC, at 300 km with a vehicle velocity of 8 km/s were compared and found to be close for the lower activation energy formation of OH(A). The agreement among the three methods was good, but in the region of peak radiation the overlay methods may overestimate the radiation by a factor of 1.5–2.0. The higher freestream number density increases the radiation rate and the freestream temperature and velocity also play important roles. Both a high freestream temperature and velocity produce collision pairs that have high collision relative velocities, which, in turn, increases the fraction of collision pairs with velocities larger than the critical velocity. For nonequilibrium flows, the reaction probability is sensitive to the number of collisions that exceed the critical velocity, so that both the freestream temperature and velocity can affect the radiation rate.

Acknowledgments

The authors would like to acknowledge support from the U.S. Air Force Office of Scientific Research Grant No. F49620-02-1-0104 administrated by Mitat Birkan and the National Science Foundation funding No. CTS-0521968. Special thanks are due to M. Ivanov of the Institute of Theoretical and Applied Mechanics, Russia for the use of the original SMILE code. We are also thankful to S. F. Gimelshein of the University of Southern California, Viterbi School of Engineering, Los Angeles, for helpful discussions.

References

[1] Chamberlain, R., Dang, A., and McClure, D., "Effect of Exhaust Chemistry on Reaction Jet Control," AIAA Paper 99-0806, Jan. 1999.

[2] Holden, M. S., Walker, B. J., Parker, R., and Bergmann, R., "Experimental Studies of Effects of Combustion on the Characteristics of Jet Interaction on Interceptor Performance in Supersonic and Hypersonic Flows," AIAA Paper 99-0808, Jan. 1999.

[3] Ebrahimi, H. B., "Numerical Simulation of Transient Jet-Interaction Phenomenology in a Supersonic Freestream," *Journal of Spacecraft and Rockets*, Vol. 37, No. 6, 2000, pp. 713–719.

[4] Kennedy, K., Walker, B., and Mikkelsen, C., "Jet Interaction Eects on a Missile with Aerodynamic Control Surfaces," AIAA Paper 99-0807, Jan. 1999.

[5] Bird, G. A., *Molecular Gas Dynamics and the Direct Simulation of Gas Flows*, Clarendon, Oxford, 1994.

[6] Tartabini, P. V., Wilmoth, R. G., and Rault, D. F. G., "Direct Simulation Monte Carlo Calculation of a Jet Interaction Experiment," *Journal of Spacecraft and Rockets*, Vol. 32, No. 6, 1995, pp. 1084–1089.

[7] Glass, C. E., and LeBeau, G. J., "Numerical Study of a Continuum Sonic Jet Interacting with a Rarefied Flow," AIAA Paper 97-2536, June 1997.

[8] Gimelshein, S. F., Levin, D. A., and Alexeenko, A. A., "Modeling of Chemically Reacting Flows from a Side Jet at High Altitudes," *Journal of Spacecraft and Rockets*, Vol. 41, No. 4, 1999, pp. 582–591.

[9] Levin, D. A., Laux, C. O., and Kruger, C. H., "A General Model for the Spectral Calculation of OH Radiation in the Ultraviolet," *Journal of Quantitative Spectroscopy and Radiative Transfer*, Vol. 61, No. 3, 1999, pp. 377–392.

[10] Gimelshein, S. F., Levin, D. A., and Drakes, J. A., "Modeling of Ultraviolet Radiation in Steady and Transient High-Altitude Plume Flows," *Journal of Thermophysics and Heat Transfer*, Vol. 16, No. 1, 2002, pp. 58–67.

[11] Li, Z., Zhong, J., and Levin, D. A., "Modeling of Radiation Events from a Side Jet Atmospheric Interaction at High Altitudes," AIAA Paper 06-3626, June 2006.

[12] Dimpfl, W. L., Light, G. C., and Bernstein, L. S., "Molecular Dynamics from Remote Observation of CO(a) from Space Shuttle Plumes," *Journal of Spacecraft and Rockets*, Vol. 42, No. 2, 2005, pp. 352–362.

[13] *GASP, The General Aerodynamic Simulation Program, Computational Flow Analysis Software for the Scientist and Engineer, User's Manual*, Ver. 3, Aerosoft Co., Blacksburg, VA, May 1996.

[14] Ivanov, M. S., Markelov, G. N., and Gimelshein, S. F., "Statistical Simulation of Reactive Rarefied Flows: Numerical Approach and Applications," AIAA Paper 98-2669, June 1998.

[15] Gimelshein, S. F., and Levin, D. A., "Modeling of Glow Radiation in the Rarefied Flow About an Orbiting Spacecraft," *Journal of Thermophysics and Heat Transfer*, Vol. 14, No. 4, 2000, pp. 471–479.

[16] Bird, G. A., "Simulation of Multi-Dimensional and Chemically Reacting Flows," *Rarefied Gas Dynamics*, Vol. 1, edited by R. Campargue, Commissariate a l'Energie Atomique, Paris, 1979, pp. 365–388.

[17] Bird, G. A., "Monte-Carlo Simulation in an Engineering Context," *Rarefied Gas Dynamics*, Vol. 74, edited by S. Fisher, AIAA, New York, 1981, pp. 239–255.

[18] Huber, K. P., and Herzberg, G., *Molecular Spectra and Molecular Structure, 4. Constants of Diatomic Molecules*, Van Nostrand Reinhold Company, New York, 1978.